Letter

Perpendicular growth of a tip-growing polymer precipitate on parallel line-patterned surfaces

Chan Jin Park [1,2] Hyobin Jeon [1] Yun Kyung Choi,[1] Ji Seon Kim [3] Young Woon Lim,[3] and Ho-Young Kim [1,4,*]

[1]*Department of Mechanical Engineering and IAMD, Seoul National University, Seoul 08826, South Korea*

[2]*Department of Chemical and Biological Engineering, Princeton University, Princeton, New Jersey 08544, USA*

[3]*School of Biological Sciences and Institute of Biodiversity, Seoul National University, Seoul 08826, South Korea*

[4]*SNU Energy Initiative, Seoul National University, Seoul 08826, South Korea*

(Received 29 December 2024; accepted 26 November 2025; published 7 January 2026)

Growth on surfaces with parallel line patterns typically results in longitudinal alignment, whether in living cells or nonliving crystals. However, unlike many other cells, tip-growing fungal germ tubes grow perpendicular to these line patterns. Here, we show that a recently reported artificial system that mimics the tip growth of germ tubes also exhibits similar perpendicular growth on grooved or ridged surfaces. Our experiments using tip-growing polymer precipitates reveal that the soft growing tip can be partially trapped by substrate patterns, and that the tip can change its growing direction when encountering the surface pattern obliquely. We theoretically rationalize this change in growth direction induced by physical interaction between the soft growing system and the substrate topography. Our physical explanation of the unique growth behavior based on material characteristics without external control suggests a way to achieve embedded physical intelligence in soft mechanical systems interacting with the surrounding objects.

DOI: 10.1103/c93s-mpwj

Surface topography can direct the growth of various systems. From living cells [1–9] to nonliving crystals [10] and self-assembling particles [11], line patterns, such as parallel grooves or ridges, usually induce longitudinal alignment. For instance, various cells, including epithelial cells, embryonic stem cells, fibroblasts, and neurons, tend to grow or migrate along such patterns [1–9]. In contrast, germ tubes of rust fungi, a large group of plant pathogenic fungi, can sense the surface morphology and grow perpendicular to these patterns [12,13]. This unique behavior results from physical interaction between the germ tube and the substrate, as it is also reproduced on chemically inert replicas of leaves [12,14,15] or even on micropatterned artificial surfaces [13,15,16]. Curiously, we observed similar perpendicular growth on line-patterned surfaces in a recently developed artificial system that mimics the tip growth of germ tubes [17]. In this Letter, we show that surface-morphology-induced perpendicular growth can be explained from the physical characteristics of tip growth.

As illustrated in Fig. 1(a), we extruded cellulose acetate-ethyl lactate-acetone solution containing red dye at a flow rate Q via a nozzle in a water-filled bath [17], over which the patterned substrate was horizontally placed. Either groove- or ridge-patterned hydrophilic foam was used as the substrate. The extruded clear solution gradually solidifies as water-contact time increases, and eventually turns into an opaque solid (see the Supplemental Material S1 [18]). While the outer layer of the precipitate solidifies, the interior remains liquid, allowing the extruded solution to flow toward the tip. Due to this replenishment, the precipitate continuously elongates from the viscoelastic tip. Upon contacting the substrate, the precipitate continues to grow from the tip along the surface. As indicated in Fig. 1(b), the growth zone (clear region), which marks the location of fresh solution, remains identical over time, maintaining a constant advancing contact angle. Particle tracking velocimetry revealed the streamlines within the growing tip [Fig. 1(c)]. Before following the tip morphology, the streamlines are skewed toward the substrate due to buoyancy, causing the growth zone to form near the substrate. When viewed from the bottom, the precipitate grew with the width identical to the tip diameter, which increased with increasing flow rate. We varied the substrate, width and depth (height) of the grooves (ridges), incident angle, size, and growth velocity of the precipitate to investigate the physical interaction-driven growth direction alignment of the tip-growing precipitates.

Perpendicular growth is observed in the tip-growing polymer precipitate when growing on a substrate patterned with either grooves or ridges. Figure 1(d) shows the precipitate encountering multiple parallel grooves during the growth. Although the precipitate first encounters the grooves obliquely, the growing direction gradually turns perpendicular to the grooves, and is maintained throughout the growth (Supplemental Material S1 [18]). The precipitate exhibits a periodic wavy shape along its length (see the Supplemental Material S2 [18]), resembling the pattern observed in germ tubes [19]. Figure 1(e) shows similar oriented growth of the precipitate on a surface with multiple ridges (Supplemental Material S2

*Contact author: hyk@snu.ac.kr

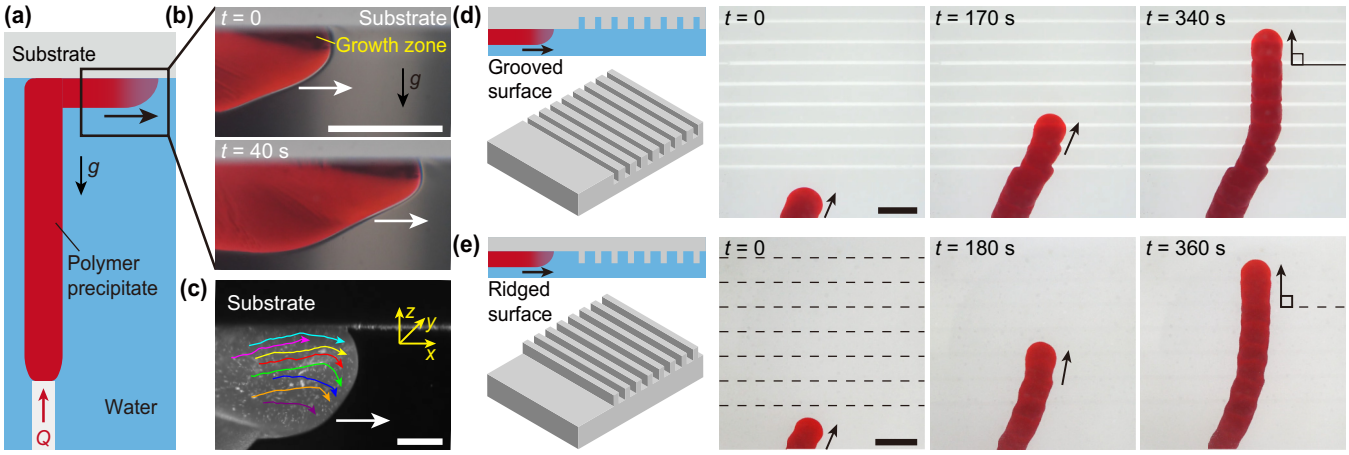

FIG. 1. (a) Schematic that depicts the side view of the experimental setup. (b) Tip growth of the precipitate on an unpatterned melamine foam. (c) Visualized internal flow in the growing tip. Oriented growth of the precipitate on grooved [panel (d)] and ridged [panel (e)] melamine foam. The ridges are denoted with dotted lines in the first image of panel (e). White [panels (b) and (c)] and black [panels (d) and (e)] arrows denote the growing direction of the precipitate. Scale bars: 1 cm [panels (b)–(e)].

[18]). This behavior is observed on two substrates with different stiffness and contact angle, suggesting minimal effect of material properties (see the Supplemental Material S3 and Table S1 [18]). We now rationalize why the growing direction of precipitates becomes aligned perpendicular to the patterns.

We start by experimentally scrutinizing how the growing precipitate interacts with a single line obstacle. The experiment was conducted on a setup similar to Figs. 1(d) and 1(e), but a single groove (ridge) was patterned, and the precipitate encountered the pattern perpendicularly. When the precipitate encountered a single groove, the tip of the precipitate got partially trapped in the groove [Fig. 2(a)]. Specifically, the region near the waist of the tip [blue circle in Fig. 2(a)] is trapped, while the apical region (green circle) crosses the groove. Partially trapped tip results in temporarily reduced width, or necking, but the precipitate continues to grow and recovers its size.

We measured the neck radius R_N varying the groove width w_g, groove depth b, and the precipitate radius R [Fig. 2(a)], to find that R_N decreases with increasing w_g for a given R since the tip gets trapped more in wider grooves [Fig. 2(b)]. Above critical w_g, the precipitate is unable to cross the groove and the whole tip gets trapped (see the Supplemental Material S4 [18]). The effect of b on R_N was found to be small (see the Supplemental Material S5 [18]).

Similar neck formation occurs when the precipitate crosses a ridge [Fig. 2(c)]. The waist of the tip gets trapped in the ridge corner and only the apical part crosses the ridge, and the precipitate recovers its size afterward. The ridge height h exerts pronounced effects on R_N, while the effect of ridge width w_r is small (see the Supplemental Material S6 [18]). The experimental results in Fig. 2(d) show that the neck width decreases with increasing ridge height.

To theoretically determine the trapped portion of the tip, we compare the distance a point in the tip can travel in the direction normal to the pattern with the characteristic length of pattern. During the growth, a material point once at the apex gradually moves along the tip in the meridional direction before being deposited at the solidifying periphery [17]. We assume that, if the point that has just made contact with the pattern can travel further than the groove width or ridge height before reaching the periphery, this point will pass the pattern. We calculate the travel distance at the growth zone. If a point at the growth zone fails to pass the pattern, the supply of replenishing solution will be cut off and this point will be unable to continue growing in the axial direction. The streamlines within the tip reveal that the velocity components in the xy plane are much greater than the z-directional component at the growth zone [Fig. 1(c)]. Thus, we used the two-dimensional (xy) velocity field in calculating the travel distance.

The travel distance normal to the pattern is the product of the velocity normal to the pattern and the growing time. We first calculate the velocity at each material point of the tip. Every point on the tip moves in the direction normal to the surface [17,20–22]. Knowing the growth direction, the growth velocity of every point at the tip can be obtained from self-similarity. As shown in Fig. 2(e), the growth velocity $u(\phi)$, where ϕ denotes the central angle, is obtained by numerically calculating the distance between the material point positions at two time steps, t_0 and t_1 (see the Supplemental Material S7 [18]). When the tip grows straight, the apex ($\phi = 0$) exhibits the maximum growth velocity U and $u(\phi)$ decreases in the meridional direction, or $u(\phi) = U f(\phi)$, where $f(\phi) = 0.0547\phi^4 - 0.553\phi^2 + 1$ is a fitted function [Fig. 2(f)] [22,23]. Knowing U and ϕ, we can calculate the normal (u_n) and tangential (u_t) components of the growth velocity with respect to the pattern. For instance, when the tip encounters the pattern perpendicularly [Fig. 2(e)], $u_n(\phi) = u(\phi)\cos\phi = U f(\phi)\cos\phi$ and $u_t(\phi) = u(\phi)\sin\phi = U f(\phi)\sin\phi$. For the timescale, we used a characteristic time of tip growth, $\tau = R/U$ (see the Supplemental Material S8 [18]) [17]. This allows us to calculate travel distance $u_n(\phi) \times \tau = R f(\phi)\cos\phi$ (see the Supplemental Material S9 [18]). According to our model, a portion near the apex has large travel distance and therefore can cross the pattern for a given

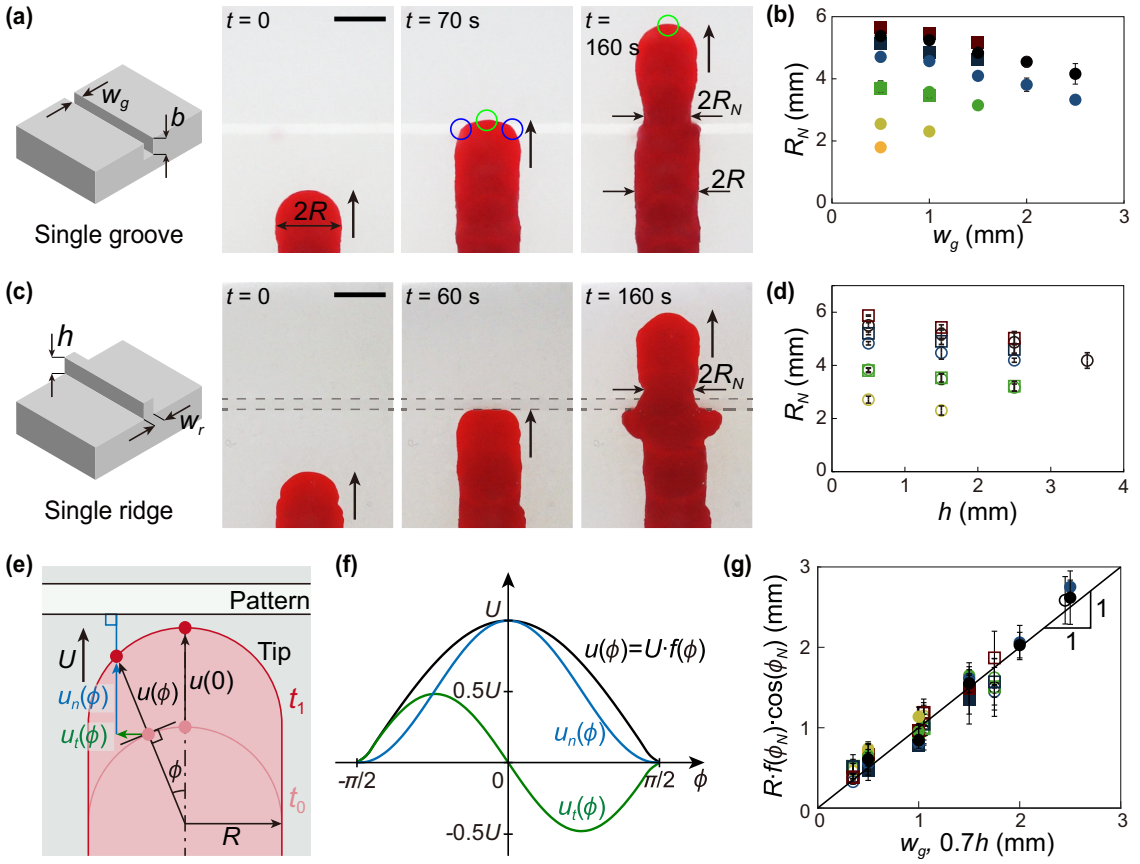

FIG. 2. (a) Tip-growing precipitate passing a single groove. (b) Neck radius R_N vs groove width w_g for precipitates with different sizes. (c) Tip-growing precipitate passing a single ridge. The ridge is denoted with dotted lines. Black arrows denote the growing direction of the precipitate [panels (a) and (c)]. Melamine foam is used as a substrate [panels (a) and (c)]. (d) Neck radius R_N vs ridge height h for precipitates with different sizes. (e) Growth velocities and growing directions at various points in the tip. (f) Calculated $u(\phi)$, $u_n(\phi)$, and $u_t(\phi)$ of a tip-growing system growing perpendicular to the pattern as shown in panel (e). (g) Experimental results shown in panels (b) and (d) are collapsed onto a single line when plotted according to our model. The symbols for different conditions are listed in Table S2 of the Supplemental Material [18] [panels (b), (d), and (e)]. Scale bars: 5 mm [panels (a) and (c)].

precipitate stream, which is consistent with the experimental finding.

We compared the travel distance in the direction normal to the pattern at the neck, $Rf(\phi_N)\cos\phi_N$, with the characteristic length scale of the pattern, where ϕ_N is the central angle at the neck. It is because the neck has the shortest normal travel distance among the points that have crossed the pattern. For the characteristic length scale of the pattern, we used the width w_g for the groove and height h for the ridge. As shown in Fig. 2(g), we found that for precipitates encountering either a groove or a ridge, the experimental results collapse onto a single line with reasonable prefactors, 1 (groove) and 0.7 (ridge).

Now we discuss how the partial trapping of tip by the pattern leads to growth direction change. Although every material point in the tip has different growth direction and velocity, the tip appears to grow in a single direction that cancels out the transverse velocity components, or $\int_{-\pi/2}^{\pi/2} u(\phi)\sin\phi \mathrm{d}\phi = 0$. Hence, we assume that a partial blockage of the growing tip causes redistribution of velocity vectors at every material point in the still-expanding region, which chooses a new growth direction that cancels out the transverse velocity components.

Figure 3(a) uses a simple vertical wall that allows us to grasp an essential physics behind such refraction of the growing tip partially blocked by an obstacle. When the growing precipitate partially contacts the obstacle, the part that has not been blocked [white solid line in the rightmost image of Fig. 3(a)] changes the growth direction (see the Supplemental Material S3 [18]). We measured the refraction angle θ_r versus the blocked meridional angle α [Fig. 3(b)]. Our assumption predicts that θ_r satisfies

$$\int_{-\pi/2+\alpha}^{\pi/2} u(\phi)\sin(\phi-\theta_r)\mathrm{d}\phi = 0, \tag{1}$$

which well matches the experimental results [Fig. 3(b); see the Supplemental Material S10 [18]].

Based on this model, we rationalize surface-morphology-induced oriented growth of tip-growing systems. When a tip is partially trapped by an obstacle, the growth direction after passing the pattern is determined by the part that is not trapped, which we can calculate using the previously described model. As shown in Figs. 3(c) and 3(d), when the tip encounters the pattern with an incident angle θ_i, if the points with a central angle ranging from $-\pi/2+\alpha$ to $\pi/2-\beta$ pass

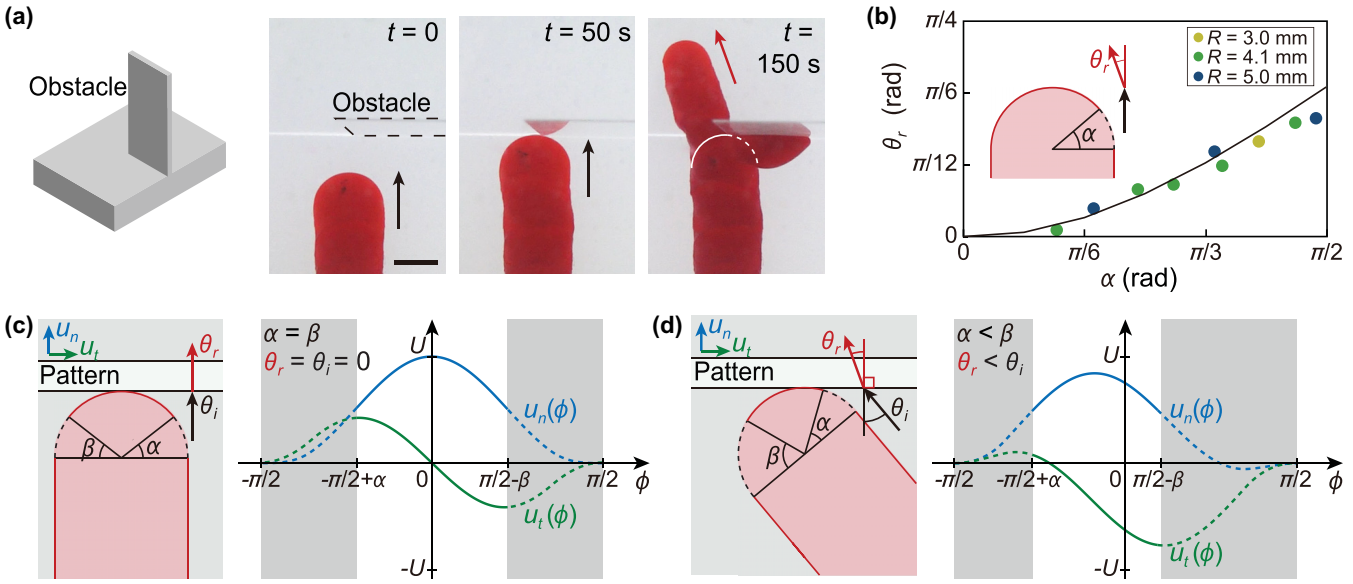

FIG. 3. (a) The growing precipitate changes the growth direction when partially blocked by a vertical wall. Black arrows and red arrow, respectively, denote the growth direction of the precipitates before and after contacting the obstacle. The outline of the obstacle is denoted with black dotted line. Scale bar: 5 mm. (b) Refraction angle after passing the obstacle. Solid line denotes theoretical prediction. Schematic of tip-growing system encountering a pattern perpendicularly [panel (c)] or obliquely [panel (d)], with corresponding growth velocity distributions. Solid lines and dotted lines, respectively, denote the nontrapped and trapped parts [panels (c) and (d)].

the pattern, the refraction angle θ_r is the angle that satisfies the following:

$$\int_{-\pi/2+\alpha}^{\pi/2-\beta} u(\phi)\sin(\phi+\theta_i-\theta_r)\mathrm{d}\phi = 0. \tag{2}$$

We consider two cases: the precipitate encountering the pattern perpendicularly or obliquely (see the Supplemental Material S11 [18]).

As shown in Fig. 3(c), when the precipitate perpendicularly encounters the pattern ($\theta_i = 0$), distribution of u_n and u_t is symmetric and the tip gets symmetrically trapped by the pattern ($\alpha = \beta$; see the Supplemental Material S12 [18]). Thus, we get $\theta_r = 0$ in Eq. (2). Therefore, when the tip-growing system perpendicularly encounters the pattern, the interaction between the pattern does not result in growth direction change ($\theta_r = 0$ when $\theta_i = 0$).

Figure 3(d) depicts a tip-growing system obliquely encountering the pattern ($\theta_i \neq 0$). In contrast to when $\theta_i = 0$, velocity distribution is not symmetric as $u_n(\phi) = u(\phi)\cos(\phi+\theta_i)$ and $u_t(\phi) = u(\phi)\sin(\phi+\theta_i)$, which results in asymmetrically trapped residue by the pattern ($\alpha < \beta$; see the Supplemental Material, S12 [18]). Due to this asymmetry, Eq. (2) yields the growth direction change after passing the pattern. Intriguingly, this asymmetry always results in the refraction angle that is smaller than the incident angle ($\theta_r < \theta_i$), since the normal velocity distribution is skewed toward $\phi = -\pi/2$.

When combined, these results rationalize the oriented growth. When a tip-growing system passes multiple line patterns, although the initial incident angle may be nonzero, the refraction angle, which is the incident angle for the next pattern, will gradually converge to zero. Once the incident

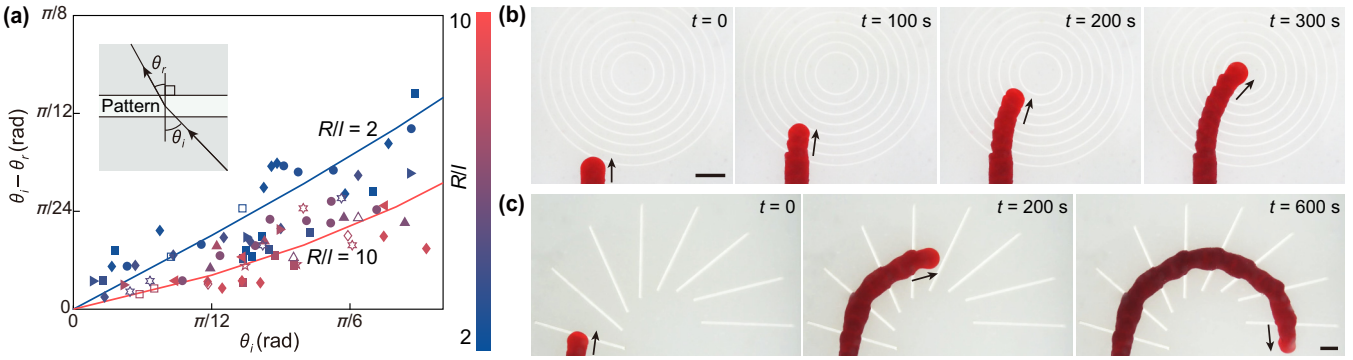

FIG. 4. (a) Growing direction change ($\theta_i - \theta_r$) of a tip-growing precipitate upon passing a line pattern. Filled and empty symbols denote precipitates encountering grooves and ridges, respectively. The symbols for different conditions are listed in Table S2 of the Supplemental Material [18]. (b) Growing precipitate grows toward the center of the bull's-eye pattern. Scale bar: 1 cm. (c) Guiding the growth of precipitate using prepatterned substrate. Scale bar: 5 mm. Black arrows denote the growing direction of the precipitate [panels (b) and (c)].

angle becomes zero, there will be no growth direction change upon passing the patterns.

Now we validate our model by comparing the theoretically predicted growth direction change ($\theta_i - \theta_r$) with the experimental results. We find that two nondimensional variables, R/l and θ_i, determine the growth direction change in the model. The growth direction change is significant when the asymmetry (difference between α and β) is large—when either R/l is small or θ_i is large. Supporting the idea that a partially blocked tip alters growth direction, both groove depth and ridge width, which minimally affect tip trapping, had little effect on the change in growth direction (see the Supplemental Material S13 [18]). As shown in Fig. 4(a), the results from the theoretical model well describe the experimental results.

Exploiting the oriented growth, we can preprogram the growth of precipitate using substrates with specific patterns. First, the growing precipitate can autonomously sense the bull's-eye pattern and change the growing direction to advance toward the pattern's center [Fig. 4(b); Supplemental Material S4 [18]]. In addition, we can precisely control the growth direction of the precipitate. For example, a substrate patterned with grooves with a specific angular arrangement can guide the precipitate to grow in a U shape [Fig. 4(c)].

Here, we demonstrated the perpendicular growth of tip-growing precipitates on surfaces with line patterns, a behavior reminiscent of tip-growing fungal germ tubes. We also rationalized how the purely physical nature of tip growth can lead to this unique behavior. While our system does not fully replicate the complex features of germ tubes, such as endocytosis or exocytosis [24], it suggests that certain behaviors of systems may emerge from the physical aspects of their growth.

We thank Professor J. Ha for critically reading the manuscript. This work was supported by National Research Foundation of Korea (Grants No. 2018-052541 and No. 2021-017476) via SNU SOFT Foundry Institute. H.-Y.K. acknowledges administrative support from SNU Institute of Engineering Research.

Data availability. The data supporting this study's findings are available within the article.

[1] A. D. Doyle, F. W. Wang, K. Matsumoto, and K. M. Yamada, One-dimensional topography underlies three-dimensional fibrillar cell migration, J. Cell Biol. **184**, 481 (2009).

[2] P. Clark, P. Connolly, A. S. G. Curtis, J. A. T. Dow, and C. D. W. Wilkinson, Topographical control of cell behaviour: II. Multiple grooved substrata, Development **108**, 635 (1990).

[3] S. Ankam, M. Suryana, L. Y. Chan, A. A. K. Moe, B. K. K. Teo, J. B. K. Law, M. P. Sheetz, H. Y. Low, and E. K. F. Yim, Substrate topography and size determine the fate of human embryonic stem cells to neuronal or glial lineage, Acta Biomater. **9**, 4535 (2013).

[4] S. A. Biela, Y. Su, J. P. Spatz, and R. Kemkemer, Different sensitivity of human endothelial cells, smooth muscle cells and fibroblasts to topography in the nano-micro range, Acta Biomater. **5**, 2460 (2009).

[5] A.-S. Andersson, P. Olsson, U. Lidberg, and D. Sutherland, The effects of continuous and discontinuous groove edges on cell shape and alignment, Exp. Cell Res. **288**, 177 (2003).

[6] K. Mukaddam, M. Astasov-Frauenhoffer, E. Fasler-Kan, L. Marot, M. Kisiel, E. Meyer, J. Köser, M. Waser, M. M. Bornstein, and S. Kühl, Effect of a nanostructured titanium surface on gingival cell adhesion, viability and properties against *P. gingivalis*, Materials **14**, 7686 (2021).

[7] P.-Y. Wang, H.-T. Yu, and W.-B. Tsai, Modulation of alignment and differentiation of skeletal myoblasts by submicron ridges/grooves surface structure, Biotechnol. Bioeng. **106**, 285 (2010).

[8] J. F. Walsh, M. E. Manwaring, and P. A. Tresco, Directional neurite outgrowth is enhanced by engineered meningeal cell-coated substrates, Tissue Eng. **11**, 1085 (2005).

[9] D. Hoffman-Kim, J. A. Mitchel, and R. V. Bellamkonda, Topography, cell response, and nerve regeneration, Annu. Rev. Biomed. Eng. **12**, 203 (2010).

[10] Y.-X. Ma and X.-D. Wang, Directional self-assembly of organic vertically superposed nanowires, Nat. Commun. **15**, 7706 (2024).

[11] A. Kaneko, Surface micro-/nanostructuring using self-assembly of fine particles, in *Micro and Nano Fabrication Technology*, edited by J. Yan (Springer, Singapore, 2018), pp. 1–28.

[12] R. Maheshwari and A. C. Hildebrandt, Directional growth of the urediospore germ tubes and stomatal penetration, Nature (London) **214**, 1145 (1967).

[13] H. C. Hoch, R. C. Staples, B. Whitehead, J. Comeau, and E. D. Wolf, Signaling for growth orientation and cell differentiation by surface topography in *Uromyces*, Science **235**, 1659 (1987).

[14] T. J. Collins and N. D. Read, Appressorium induction by topographical signals in six cereal rusts, Physiol. Mol. Plant Pathol. **51**, 169 (1997).

[15] N. D. Read, L. J. Kellock, T. J. Collins, and A. M. Gundlach, Role of topography sensing for infection structure differentiation in cereal rust fungi, Planta **202**, 163 (1997).

[16] E. A. Allen, *et al.*, Appressorium formation in response to topographical signals by 27 rust species, Phytopathology **81**, 323 (1991).

[17] C. J. Park, J. Ha, H.-R. Lee, K. Park, J.-Y. Sun, and H.-Y. Kim, Plant cell-like tip-growing polymer precipitate with structurally embedded multistimuli sensing ability, Proc. Natl. Acad. Sci. USA **120**, e2211416120 (2023).

[18] See Supplemental Material at http://link.aps.org/supplemental/10.1103/c93s-mpwj for additional experimental characterizations and detailed derivations of the models.

[19] N. D. Read, L. J. Kellock, H. Knight, and A. J. Trewavas, Contact sensing during infection by fungal pathogens, in *Perspectives in Plant Cell Recognition*, edited by J. A. Callow and J. R. Green (Cambridge University Press, Cambridge, UK, 1992), pp. 137–172.

[20] A. Goriely and M. Tabor, Self-similar tip growth in filamentary organisms, Phys. Rev. Lett. **90**, 108101 (2003).

[21] S. Bartnicki-García, C. E. Bracker, G. Gierz, R. López-Franco, and H. Lu, Mapping the growth of fungal hyphae: Orthogonal cell wall expansion during tip growth and the role of turgor, Biophys. J. **79**, 2382 (2000).

[22] O. Campàs and L. Mahadevan, Shape and dynamics of tip-growing cells, Curr. Biol. **19**, 2102 (2009).

[23] J. Dumais, S. L. Shaw, C. R. Steele, S. R. Long, and P. M. Ray, An anisotropic-viscoplastic model of plant cell morphogenesis by tip growth, Int. J. Dev. Biol. **50**, 209 (2006).

[24] M. Riquelme, J. Aguirre, S. Bartnicki-García, G. H. Braus, M. Feldbrügge, U. Fleig, W. Hansberg, A. Herrera-Estrella, J. Kämper, U. Kück, R. R. Mouriño-Pérez, N. Takeshita, and R. Fischer, Fungal morphogenesis, from the polarized growth of hyphae to complex reproduction and infection structures, Microbiol. Mol. Biol. Rev. **82**, e00068-17 (2018).

Supplementary Information for
Perpendicular growth of a tip-growing polymer precipitate on parallel line-patterned surfaces

Chan Jin Park, Hyobin Jeon, Yun Kyung Choi, Ji Seon Kim, Young Woon Lim, and Ho-Young Kim*

*Email: hyk@snu.ac.kr

This PDF file includes:

Materials and Methods

Supplementary Discussions S1 to S13

Tables S1 and S2

Legends for movies S1 to S4

Other supplementary materials for this manuscript include the following:

Movies S1 to S4

Materials and Methods

Materials

For every experiment, polymer solution was prepared by dissolving cellulose acetate (Sigma-Aldrich, average Mn 30,000) in mixture of ethyl lactate (Sigma-Aldrich) and acetone. Oil Red O (Sigma-Aldrich) was added to the polymer solution to facilitate visualization. The composition of the solution was 24.9 wt% cellulose acetate, 0.1 wt% Oil Red O, 25 wt% ethyl lactate, and 50 wt% acetone. Prepared polymeric solution was extruded using a syringe pump (LSP04-1A, Longer Precision Pump). When visualizing the internal flow, fluorescent polystyrene particles (PS-FluoRed-10) of average diameter of 10 μm was added to the solution. Hydrophilic melamine foam (Samjeong) and PVA foam (Cleantek) were used as the substrate, where the patterns generated from Adobe Illustrator were engraved using a laser cutter. Due to the difference in the advancing contact angle of the precipitate on melamine foam and PVA foam (Table S1), the precipitate growing on PVA foam exhibited larger size (R) and a lower growing velocity (U) when extruded at an identical flow rate (Table S2).

Experimental setup

The polymer solution was extruded at a fixed flow rate using a syringe pump in a water-filled bath, over which the patterned substrate was placed horizontally. As the solvent of the solution dissolved into the surrounding water, the consequent precipitate of cellulose acetate initially grew against gravity due to buoyancy. Once it touched the substrate, it grew along the solid surface, still elongating only at the tip. Before the precipitate contacted the substrate, an external flow along the surface was briefly applied using a syringe. This induced flow guided the precipitate to grow in the same direction as the applied flow, allowing control over the incident angle between the precipitate and the obstacle. The growth of precipitate was recorded using a video camera positioned beneath the water bath.

Substrate stiffness measurement

Using a universal testing machine (34SC-1, Instron), we applied a load to a fully wet substrate using a spherical steel indenter with a diameter of 500 μm and measured the resulting deformation of the substrate. According to the Hertzian contact model, when a sphere of radius R_i is pressed

into a soft material, the indentation force F is related to the indentation depth, δ by

$$F = \frac{4}{3} E^* \sqrt{R_i} \delta^{3/2}. \tag{S1}$$

Here E^* is the effective modulus defined as

$$\frac{1}{E^*} = \frac{1 - {\nu_i}^2}{E_i} + \frac{1 - {\nu_s}^2}{E_s}, \tag{S2}$$

where ν and E are Poisson's ratio and Young's modulus, respectively, and the subscripts i and s refer to the indenter and substrate, respectively. We used $\nu_i = 0.3$, $E_i = 200$ GPa, and $\nu_s = 0.5$ to obtain Young's modulus of the substrate E_s.

S1. Tip growth of polymer precipitate in water and on a solid surface

When the polymer solution is extruded through the nozzle into water, solvent (acetone and ethyl lactate)–non-solvent (water) exchange occurs. As a result, the extruded clear polymer solution gradually turns into an opaque solid as the solvent diffuses out and non-solvent diffuses in. Upon contact with the water, the outer layer of the solution rapidly turns into a gel-like aggregate. However, because solvent–non-solvent exchange is a diffusion-driven process, the interior remains liquid, allowing the solution to flow toward the tip. The extrusion process provides high internal pressure, which causes the expansion of the viscoelastic tip, or growth. Since this expansion is driven by pressure, each material point at the tip always moves in a direction normal to the surface. Expansion is greatest at the apex of the tip and decreases along the meridional direction, eventually ceasing at the solidified waist. This gradient of expansion occurs because the polymer solution gradually solidifies as water contact time increases, which also increases along meridional direction.

Once the tip-growing polymer precipitate, which initially grows in the direction of buoyancy in liquid, contacts the substrate, the precipitate continues to grow from the tip, but grows along the solid surface. The growing direction of the precipitate, once determined upon contact with the substrate, remains unchanged in the absence of external intervention. As shown in Fig. 1(b), at the tip, the shape of the clear region, or growth zone, where fresh solution is replenished and growth occurs, remains identical over time. Fig. S1 shows the side view images of the precipitates extruded at different flow rates, growing on a flat hydrophilic melamine foam. With increasing flow rate, the size and the growing velocity of the precipitate increases (Supplementary table S2), yet the contact angle at the tip remains identical.

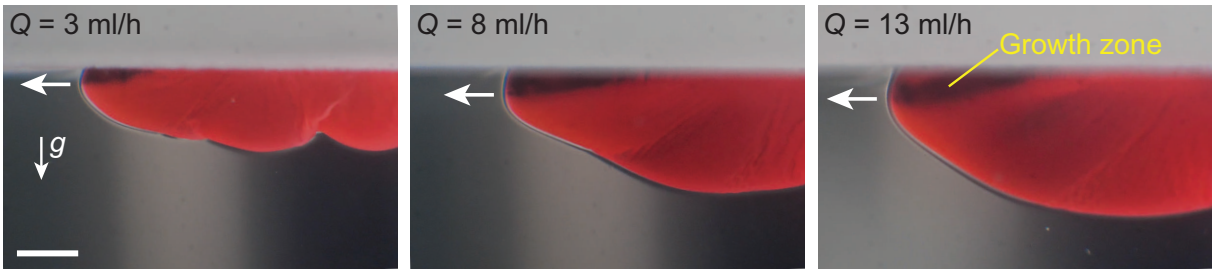

FIG. S1: **Side view images of precipitate extruded at different flow rates.** Size of the precipitate increases with increasing extrusion flow rate, but the contact angle at the tip remains constant. The elongation only occurs at the growth zone at the tip, which appears dark. White arrows denote the growing direction of the precipitate. Scale bar, 5 mm.

As shown in Fig. S2, the thickness of outer layer in the growing tip, which rapidly turns into a gel-like aggregate and act as a wall, is small at the growth zone near the apex of the tip (small water-contact time) and increases along the axial direction (with increasing water-contact time) as the precipitation is diffusion-driven process.

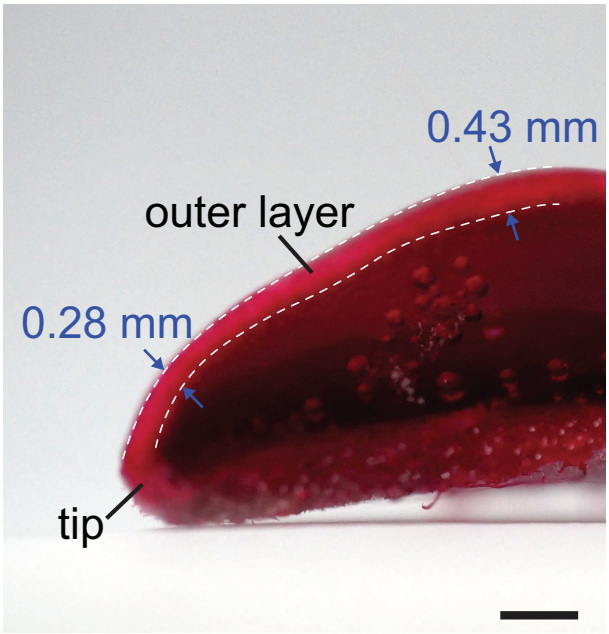

FIG. S2: **Outer layer thickness distribution at the tip.** Outer layer thickness is smallest at the growing tip and increases along the axial direction. Scale bar, 1 mm.

S2. Wavelength of the precipitate growing on grooved substrates are identical to that of the pattern

When growing on grooved substrates, the precipitate exhibits a periodic wavy shape with the wavelength, $\lambda_{\text{precipitate}}$, identical to that of the pattern, λ_{pattern} as shown in Fig. S3. The trough of the shape is always located at where the precipitate exits the groove. Similar shapes have also been reported in the tip-growing germ tubes growing on a grooved substrate.

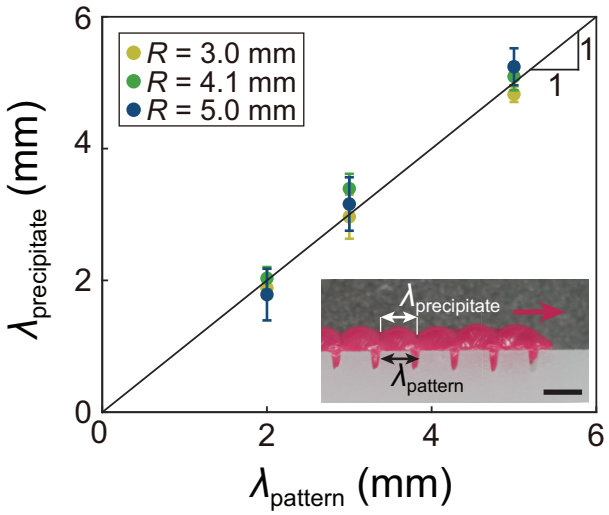

FIG. S3: **Wavelengths of precipitate growing on grooved substrates are identical to that of the pattern.** Regardless of its size, the wavelength of the precipitate is always identical to that of the pattern. Red arrows denote the growing direction of the precipitate. Scale bar, 5 mm.

S3. Perpendicular growth of precipitate on line-patterned PVA foams

Similar to experiments on patterned melamine foams (Figs. 1d and e), perpendicular growth of precipitate was observed on PVA foam patterned with either grooves or ridges (Fig. S4). Large difference in the measured stiffness of the two substrate materials – differing by two orders of magnitude – suggests that material properties have an insignificant effect on the observed perpendicular growth (Supplementary table S1).

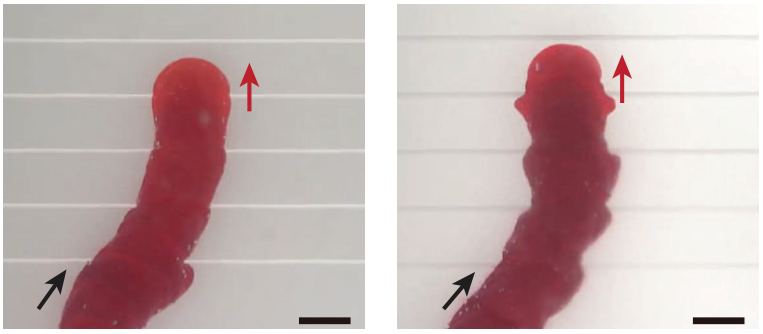

FIG. S4: **Perpendicular growth of precipitate on line-patterned PVA foams.** Perpendicular growth is observed on both groove patterned (left) and ridge patterned (right) PVA foams. Black and red arrows denote initial and aligned growing direction, respectively. Scale bars, 5 mm.

S4. Critical groove width and ridge height allowing the precipitate to pass

When the precipitate encounters a groove too wide, or a ridge that is too high, the whole tip gets trapped by the pattern. We experimentally determined the critical groove width and ridge height allowing the precipitate to pass, by growing the precipitate on substrates with grooves of varying width or ridges of varying height. As shown in Fig. S5, the critical groove width or ridge height increased with increasing precipitate size. For instance, critical groove width is approximately a half of the tip radius and critical ridge height is approximately two thirds of the tip radius.

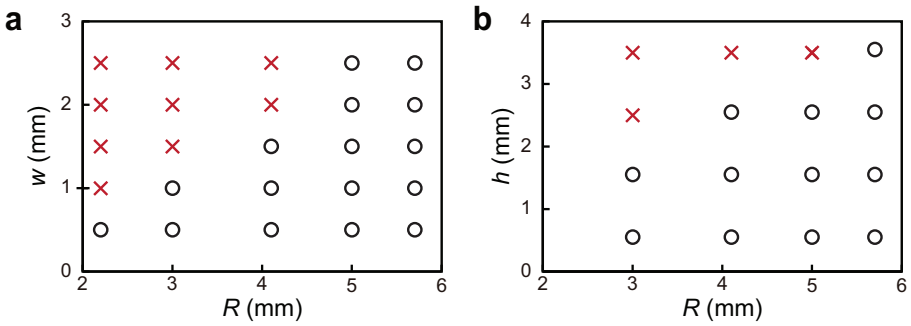

FIG. S5: **Critical groove width and ridge height that a precipitate can pass.** The behavior of the precipitate after encountering a groove (**a**) or a ridge (**b**). Black circles denote that the precipitate can pass the pattern, while red crosses denote that the whole tip gets trapped. Critical groove width or ridge height which the precipitate can pass increases with increasing precipitate size. We conducted the experiment at least thrice for each experimental condition.

S5. Effect of groove depth on necking of precipitate

We tested the effect of groove depth on the behavior of a growing precipitate in contact with grooves of varying depth. We experimentally found that whether the precipitate can cross the groove or not is not affected by the depth of the groove, but determined by the width of the groove. However, the groove depth affected the behavior of the portion of precipitate that has been trapped by the pattern. As shown in the left image of Fig. S6, when the precipitate encounters a shallow groove (b = 2 mm), the trapped portion grows along the groove after reaching the trough bottom. On the other hand, as shown in the right image of Fig. S6 , when the groove is sufficiently deep (b = 4 mm), the growth of trapped part is ceased before it reaches the trough bottom. Therefore, in contrast to when encountering the shallow groove, trapped part growing along the pattern, is not visible. However, despite the difference in the depth, the precipitates exhibit similar neck radius upon passing the obstacle.

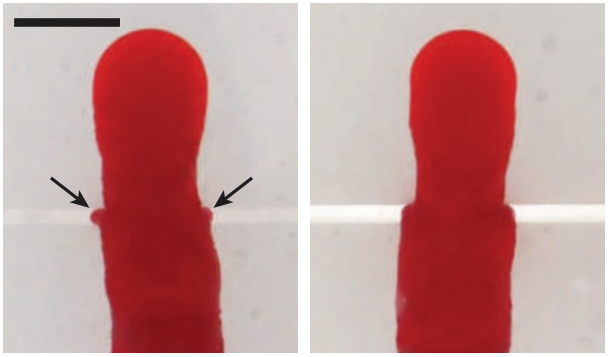

FIG. S6: **Effect of groove depth.** Images of precipitates encountering shallow (left, b = 2 mm) and deep (right, b = 4 mm) groove. Black arrows in the left image show the trapped part growing along the groove after reaching the trough bottom. Scale bar, 5 mm.

S6. Necking of precipitate when encountering a plateau

To test the effect of ridge width on neck formation, we made the precipitate to encounter a plateau, which represents a ridge with infinite width. As shown in Fig. S7, consistent with precipitates encountering a ridge, we observed necking. In addition, increasing the plateau height (right image of Fig. S7) decreased the neck radius as a larger portion of the tip became trapped. These results imply that neck forms when the precipitate ascends either a ridge or plateau, which is the result of the tip getting partially blocked by the obstacle. Therefore, the effect of ridge width on the growth of precipitate is small.

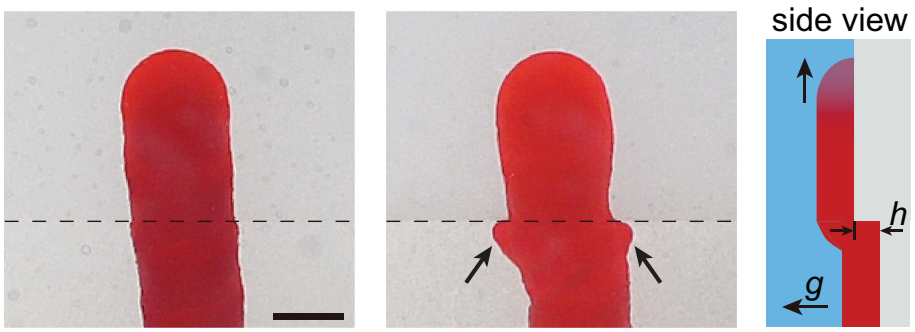

FIG. S7: **Necking of precipitate when encountering plateaus with different height.** Images of precipitates encountering shallow (left, h = 0.5 mm) and tall (right, h = 2 mm) plateau. Black dotted lines denote the boundary of the plateau. Black arrows in the right image show the trapped part at the plateau boundary. Scale bar, 5 mm.

S7. Calculation of growing velocity

The growing velocity at each point of the tip is obtained by numerically calculating the distance traveled by a material point over a given time interval. As shown in Fig. S8, the growing precipitate can be modeled to consist of a semicircular tip attached to a rectangular stalk at the interface with the substrate. Although the tip appears to undergo translational motion with a velocity of U in the growing direction, each material point on the tip moves in the direction normal to the surface as the growth is driven by pressure.

We assume that the precipitate advances a distance $d = s(0)$ in the growth direction from time t_0 to t_1, where $s(\phi)$ is the distance traveled by a material point at a central angle ϕ. The position of an arbitrary material point at time t_1 is the intersection of its normal vector at time t_0 with the precipitate at t_1. Therefore, we can numerically calculate the distance traveled by a material point at the tip, $s(\phi)$, during this time interval. Since the travel distance of the point is related to the growing velocity, which is U at the apex of the tip ($\phi = 0$), we can calculate the growing velocity at each point, $u(\phi) = Us(\phi)/d$. For U, we use experimentally measured values from precipitates growing on a flat substrate

If d is too large, the intersection point of normal vector at time t_0 and precipitate at t_1 can be located at the stalk rather than the tip in the points very close to the periphery. However, when the advanced distance normalized by the tip radius during the interval, d/R, is smaller than 0.1, this effect becomes insignificant. Considering that the growing velocity of the whole tip is small, $U \sim \mathrm{O}(10^{-4})$ m/s, we numerically obtained the growing velocity with the interval corresponding to $d/R = 0.1$. We then fitted this curve $u(\phi) = Uf(\phi)$ and obtained $f(\phi) = 0.0547\phi^4 - 0.553\phi^2 + 1$, which gave R-squared value of $R^2 = 0.999$. Since the growth of precipitate at the tip is self-similar (shape of the growth zone remains identical over time; Fig. 1b), we assumed that $u(\phi)$ is time-independent.

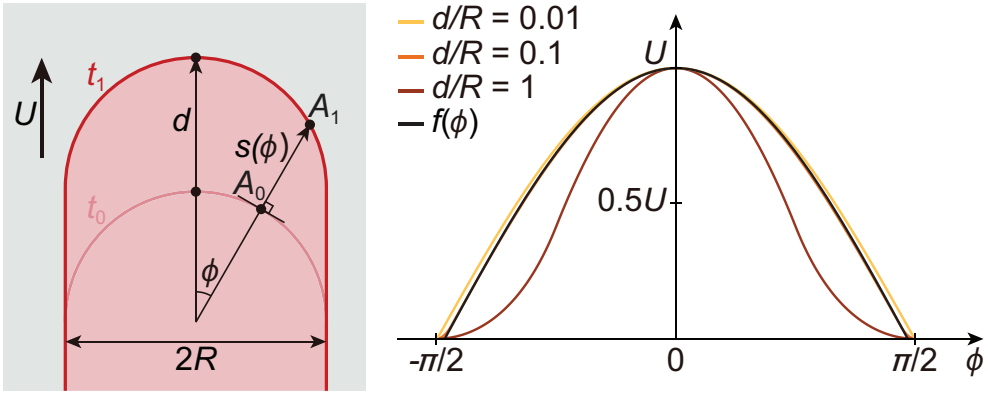

FIG. S8: **Distribution of growing velocity for different d/R.** Distribution of growing velocity is calculated from the distance traveled by a material point over a given time interval. Material point A_0 at time t_0 moves to A_1 at time t_1. As long as d/R is small (< 0.1), the velocity profiles are independent of d/R.

S8. Characteristic time scale

In the tip-growing precipitates, both the tip radius R and the growing velocity at the apex U are altered with varying extrusion flow rate Q. Therefore, we can define a characteristic time scale $\tau = R/U$, which scales the time that a material point moves from the apex to the periphery of the tip. As shown in Fig. S9, we have experimentally measured τ while varying Q. We have found that τ increases with the increasing Q in our experimental conditions (Q = 3 to 20 ml/h)

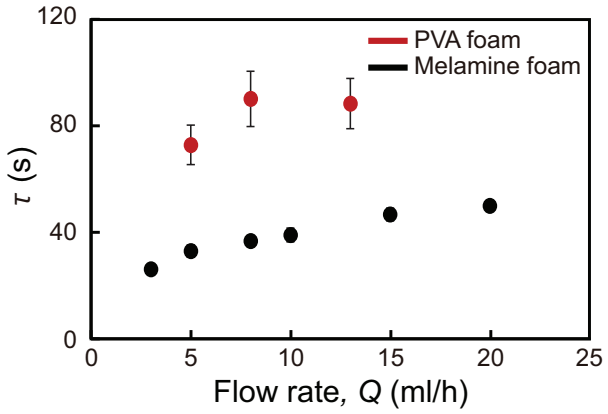

FIG. S9: **Characteristic time scale τ versus extrusion flow rate Q.** τ is experimentally found to increase with increasing Q.

S9. Detailed derivation of the model predicting the portion of the tip that gets trapped by the pattern

To calculate the part of the tip gets trapped by the pattern, we compare the travel distance of a material point at the tip, in the direction normal to the pattern, with the characteristic length of the pattern. Our assumption was that the points with a travel distance smaller than the characteristic length would be unable to cross the pattern and become trapped by the pattern. In developing the model, we assumed that whether the point at the growth zone of the precipitate and the substrate travels far enough to cross the pattern is critical. This assumption was based on the fact that if this point initially at the tip fails to cross the pattern, the fresh polymer solution, which is necessary for the point's continued growth, will be cut off. Additionally, since the streamlines are nearly parallel to the surface at the growth zone, forming a small angle of approximately 10°, we neglected the transverse component and considered only the planar components of the velocity at the interface.

Calculating the travel distance requires information on growing velocity and time scale associated with the growth. Since the tip advances with a nearly constant velocity, and every material point move in the direction normal to the surface, we can determine the growing velocity at every point at the tip. The detailed process of growing velocity calculation is shown in Supplementary discussion S7. From this calculation, we obtain the growing velocity $u(\phi) = Uf(\phi)$, where U is experimentally obtained and $f(\phi) = 0.0547\phi^4 - 0.553\phi^2 + 1$ is a fitted function. Knowing $u(\phi)$ allows us to calculate the velocity component normal to the pattern. For instance, if the precipitate perpendicularly encounters the pattern as shown in Fig. 2(e), the velocity normal to the pattern is $u_n(\phi) = Uf(\phi)\cos\phi$. In the tip-growing precipitate, the size of the growing precipitate R and advancing velocity of the tip U set a characteristic time of growth $\tau = R/U$, which indicates how long a material point can move before being deposited at the waist of the tip.

Knowing the growing velocity and time scale of growth, we can calculate the travel distance normal to the pattern, which is $u_n(\phi) \cdot \tau = (Uf(\phi)\cos\phi) \cdot (R/U) = Rf(\phi)\cos\phi$. This suggests that the travel distance in the direction normal to the pattern can be described using purely geometric variables R and ϕ. As shown in Fig. 2(g), we compared theoretical travel distance at the neck, which is the point that has smallest normal travel distance among the points that have crossed the pattern, and found that the model well describes the experimental data. Due to the

shape of $f(\phi)$ (Supplementary discussion S7) and $\cos\phi$, the travel distance is large near the apex of the tip and becomes smaller as approaching the waist. Therefore, the experimental observation that points closer to the waist than the neck fail to cross the pattern qualitatively matches the model's prediction.

As shown in Table S2, the substrate material affects the size and the growing velocity of the precipitate. Specifically, precipitates growing on PVA foam, which has lower advancing contact angle than melamine foam, have a larger R and therefore lower U at identical extrusion flow rate. However, the fact that the data from these two different substrates collapses onto a single curve derived from the model implies that in our system, variables related to geometry are critical in determining whether the point will cross the pattern or not.

S10. Growth simulation after partial blockage

When a tip of the growing precipitate is partially blocked by an obstacle – either a simple vertical wall or a line pattern – the unblocked part changes growing direction. We assumed that the new growing direction of the continuously growing part is the direction that cancels out the tangential components of the velocity, which is the case in tip-growing systems growing straight without external intervention. To test this assumption, we compared shape of simulated growth under this condition with experimental results.

In the simulation, the material point with central angle ϕ at time $t = i$ moved in the direction normal to the surface by a distance $s(\phi)$, determining its position at $t = i + 1$. Once a point reached the periphery ($\phi < -\pi/2$ or $\phi > \pi/2$), it stopped moving, and a new point was inserted at the midpoint between the two points with the largest separation to maintain a constant number of points. The inputs to the simulation were the initial positions of the material points and the distribution of $s(\phi)$. For $s(\phi)$, we used the profile shown in Fig. S8 with $s(0) = R/6$ to ensure notable growth per time step.

We assumed a situation where the precipitate, which initially grows straight, is partially blocked at the tip at $t = 0$ in the range of $-\pi/2 < \phi < -\pi/12$, which is set to match the experiment. Based on Eq. (1), the growth direction change in the unblocked part, or refraction angle, was $\pi/9$. To account for this change, we shifted $s(\phi)$ by $\pi/9$ at $t = 0$, so that the material point at $\phi = \pi/9$ now moves a distance of $R/6$. From $t = 1$, the point at the apex exhibited the maximum displacement, following the distribution of $s(\phi)$ shown in Fig. S8. Fig. S10 shows the simulated growth alongside the corresponding experimental results. Although there is a brief delay before the growth direction change actually takes place in the experiment ($t = 30$ s), the similarity in the shapes between the simulation and the experiment supports the validity of our assumption.

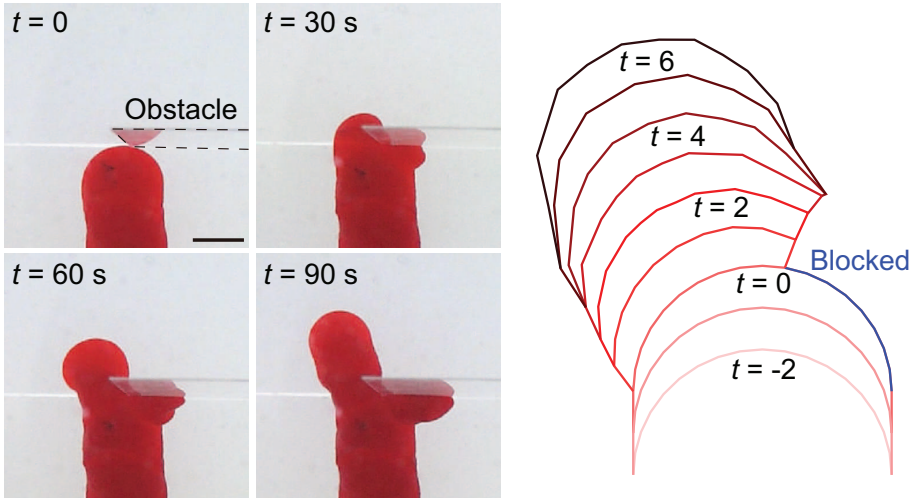

FIG. S10: **Comparison of experiment and growth simulation after partial tip blockage.** Tip is partially blocked at $t = 0$ in both experiment and simulation. Scale bar, 5 mm.

S11. Detailed derivation of the model predicting the growth direction after encountering a line pattern

After an oblique encounter with a line pattern – either a groove or a ridge – the non-trapped part of the tip that has crossed the pattern changes growing direction. In contrast, although partial trapping of the tip is still observed, perpendicular encounter does not results in growth direction change. In the tip-growing system, although every material point at the tip grows in different directions (direction normal to the surface at each point), the tip as a whole advances in a single direction, which is the direction that cancels out the tangential components of the velocity. Based on this characteristic, we assumed that the new growing direction is determined by the part that has passed the pattern, which is the direction that cancels out the tangential components of the growing velocity in the non-trapped part. We also assumed that the precipitate continues to grow in this changed direction even after recovering its original size. Letting points with central angle ranging from $-\pi/2 + \alpha < \phi < \pi/2 - \beta$ passes the pattern, the predicted direction is then the direction that satisfies Eq. (2) in the manuscript. To test our assumption, we partially blocked the tip using a vertical wall and compared the predicted growth direction change, or refraction angle, based on our assumption with experimental results (Figs. 3a, b). We also compared the dynamic shape change of the tip based on our assumption with the experimental results (Supplementary discussion S10). In both experiments, the prediction from the model well described the experimental results, which supports the assumption.

Calculating the new direction requires information on α and β, which are the polar angle of the trapped part in either halves of the tip (points at the tip with polar angle ranging from $-\pi/2 < \phi < -\pi/2 + \alpha$ and $\pi/2 - \beta < \phi < \pi/2$ gets trapped by the pattern). To obtain α and β, we use the previously described model, which calculates the trapped part of the tip by comparing travel distance normal to the pattern with the characteristic length of the pattern. The input of the calculation is the size of the precipitate R, characteristic length of the pattern l, and incident angle θ_i, where $l = w_g$ for the groove, and $l = 0.7h$ for the ridge. We solve the equation $Rf(\phi)\cos(\phi + \theta_i) = l$ for ϕ in the range of $[-\pi/2, \pi/2]$, which gives two solutions α and β. Then, α and β are used as a input in Eq. (2) to numerically calculate the new growing direction, or refraction angle, θ_r.

Similar to Figs. 2(a) and (c), when the precipitate perpendicularly encounters a line pattern

($\theta_i = 0$), the tip gets symmetrically trapped ($\alpha = \beta$) because both the functions $f(\phi)$ and $\cos\phi$ are symmetric about $\phi = 0$. For instance, when $R = 4.3$ mm, $w_g = 1$ mm, and $\theta_i = 0$, we get $\alpha = \beta = \pi/6$. Numerical calculation always gives $\theta_r = 0$, which we can also prove conceptually. Before the encounter with the pattern, the precipitate grows in the direction that cancels out the tangential components, so $\int_{-\pi/2}^{\pi/2} u(\phi)\sin\phi \mathrm{d}\phi = 0$ is satisfied. Since $u(\phi) = Uf(\phi)$ is symmetric about $\phi = 0$ (even function) and $\sin\phi$ is antisymmetric about $\phi = 0$ (odd function), the product of these two, which is the integrand, is antisymmetric about $\phi = 0$. Based on this antisymmetry, we can write $\int_{-\pi/2}^{\pi/2} u(\phi)\sin\phi \mathrm{d}\phi = \int_{-\pi/2+\alpha}^{\pi/2-\alpha} u(\phi)\sin\phi \mathrm{d}\phi = \int_{-\pi/2+\alpha}^{\pi/2-\beta} u(\phi)\sin\phi \mathrm{d}\phi = 0$ if $\alpha = \beta$. This implies that $\theta_r = 0$ satisfies Eq. (2).

When the precipitate obliquely encounters a line pattern ($\theta_i \neq 0$), the tip is no longer symmetrically trapped because $\cos(\phi + \theta_i)$ is not symmetric about $\phi = 0$. Still, we can numerically obtain α and β. For instance, when $R = 4.3$ mm, $w_g = 1$ mm, and $\theta_i = \pi/6$, we get $\alpha = \pi/9$ and $\beta = 4\pi/15$. Numerically solving Eq. (2) using the obtained α and β, we get $\theta_r = \pi/9$. As shown in Fig. 3d, because the normal velocity distribution is skewed towards $\phi = -\pi/2$, α, which is the trapped part of the tip in the half that encounters the pattern first, is always smaller than β. Since $\alpha < \beta$, we always get $\theta_r < \theta_i$, which rationalizes why the growing direction becomes more perpendicularly oriented after passing the pattern. Experimental evidences of symmetrical and asymmetrical trap of tip upon pattern encounter is shown in Supplementary discussion S12.

S12. Symmetrical and asymmetrical trap of tip

As described in Figs. 3(c) and (d), the model predicts that the tip is symmetrically trapped when the tip-growing system encounters the pattern perpendicularly. On the other hand, the model predicts that the tip is asymmetrically trapped when encountering the pattern obliquely, with the half that encounters the pattern relatively later being more trapped. To verify whether the model correctly describes the experimental results, we observed the trapped portion of the precipitate.

We first observed cross sections of the precipitate that has passed multiple grooves. As shown in Fig. S11(a), the following two sections were imaged: when the precipitate encountered the groove perpendicularly ($\theta_i = 0$, cross section A-A^{-}) and obliquely ($\theta_i \neq 0$, cross section B-B^{-}). While the trapped residue is nearly symmetric in the cross section A-A^{-}, it is asymmetric in cross section B-B^{-}. Also, in section B-B^{-}, the trapped residue near point B (thus meeting the groove earlier) is significantly smaller than the trapped residue near point B^{-} (thus meeting the groove later).

We also investigated the results from the precipitate that has passed multiple ridges. In agreement with our theoretical model, as shown in Fig. S11(b), when the precipitate encounters the ridge perpendicularly, the tip is nearly symmetrically trapped (upper red and blue arrows). On the other hand, when the precipitate encounters the ridge obliquely, the portion of tip that has encountered the groove first (lower red arrow) leaves a much smaller residual than the trapped residual of the tip portion that has encountered the ridge later (lower blue arrow).

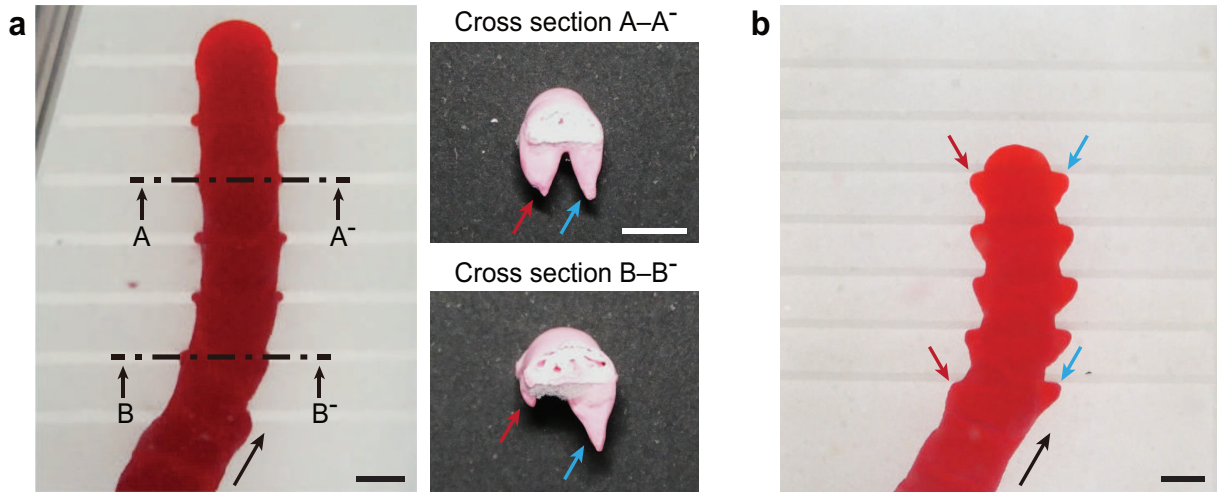

FIG. S11: **Shape of trapped parts.** **a**, Trapped parts of the tip when the precipitate encounters multiple grooves. Cross section A-A' denotes when the precipitate encounters the groove perpendicularly, and section B-B' denotes when the precipitate encounters the groove obliquely. **b**, Trapped parts of the tip when the precipitate encounters multiple ridges. The red arrows denote the trapped part in the left half (the half that encounters the pattern first when obliquely encountering the pattern), and the blue arrows denote the trapped part in the right half (**a, b**). Scale bars, 5 mm.

S13. Effect of groove depth and ridge width on growth direction change

Experiments using a simple vertical wall indicate that partial blockage of the tip changes the growing direction of the precipitate. To confirm this idea, we measured changes in growing direction of precipitates while varying the groove depth or ridge width. Since neither groove depth nor ridge width affects the trapping of the tip, we expected that changing these variables will only have a minor effect on the growing direction of the precipitate.

Fig. S12(a) shows precipitates encountering either shallow or deep grooves at similar incident angles. Other variables including groove width, groove spacing, precipitate size, and growing velocity are identical. The change in growth direction is similar regardless of the groove depth. Similarly, ridge width has little effect on the change in growth direction. For instance, in Fig. S12(b), regardless of the ridge width, the growth of precipitate becomes perpendicularly aligned after passing two ridges, and a perpendicular encounter with a ridge does not alter the growing direction.

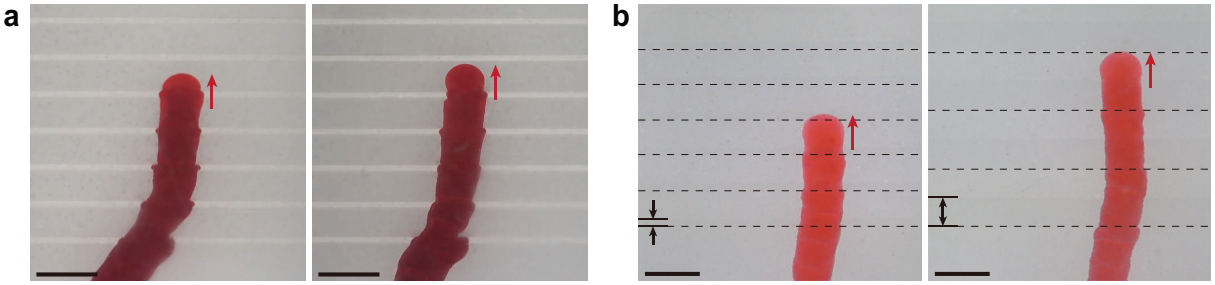

FIG. S12: **Groove depth or ridge width do not affect the growth direction change of the precipitate.** **a**, A similar change in growing direction is observed when passing grooves with depths of 2 mm (left) and 4 mm (right). **b**, A similar change in growing direction is observed when passing ridges with widths of 1 mm (left) and 5 mm (right). Black arrows denote the width of the first ridge that a precipitate encounters, and black dotted lines denote the leading edges of ridges. Red arrows denote the growing direction of the precipitates (**a, b**). Scale bars, 1 cm (**a, b**).

Table S1. Material properties of substrates

Substrate	Stiffness (Pa)	Advancing contact angle (°)
Melamine foam	2,892.9	120
PVA foam	31.8	75

Table S2. List of precipitate sizes, growing speeds, and symbols. Precipitate size and growing speed are given for a specific extrusion flow rate. Values are the average and standard deviation from at least three measurements.

Substrate	Flow rate (ml/h)	Precipitate size, R (mm)	Growing speed, U (μm/s)	Symbol	
				Fig. 2	Fig. 4
Melamine foam	3	2.2 ± 0.057	84 ± 4	●	
	5	3.0 ± 0.062	91 ± 6	●	●
	8	3.6 ± 0.054	98 ± 4		■
	10	4.1 ± 0.191	105 ± 5	●	◆
	15	5.0 ± 0.099	107 ± 5	●	✸
	20	5.7 ± 0.092	114 ± 3	●	★
PVA foam	5	4.3 ± 0.034	59 ± 6	■	▲
	8	5.5 ± 0.071	61 ± 7	■	▶
	13	6.1 ± 0.21	69 ± 7	■	◀

Movie legends

Movie S1. Surface-morphology-induced oriented growth of polymer precipitate on a grooved substrate.

Movie S2. Surface-morphology-induced oriented growth of polymer precipitate on a ridged substrate.

Movie S3. Change in growth direction of polymer precipitate when the tip is partially blocked by an obstacle.

Movie S4. Polymer precipitate grows towards the center when growing on a bull's-eye patterned substrate.